JAAS

Accepted Manuscript

This is an *Accepted Manuscript*, which has been through the Royal Society of Chemistry peer review process and has been accepted for publication.

Accepted Manuscripts are published online shortly after acceptance, before technical editing, formatting and proof reading. Using this free service, authors can make their results available to the community, in citable form, before we publish the edited article. We will replace this *Accepted Manuscript* with the edited and formatted *Advance Article* as soon as it is available.

You can find more information about *Accepted Manuscripts* in the Information for Authors.

Please note that technical editing may introduce minor changes to the text and/or graphics, which may alter content. The journal's standard Terms & Conditions and the Ethical guidelines still apply. In no event shall the Royal Society of Chemistry be held responsible for any errors or omissions in this *Accepted Manuscript* or any consequences arising from the use of any information it contains.

ROYAL SOCIETY OF CHEMISTRY

www.rsc.org/jaas

Graphical Abstract

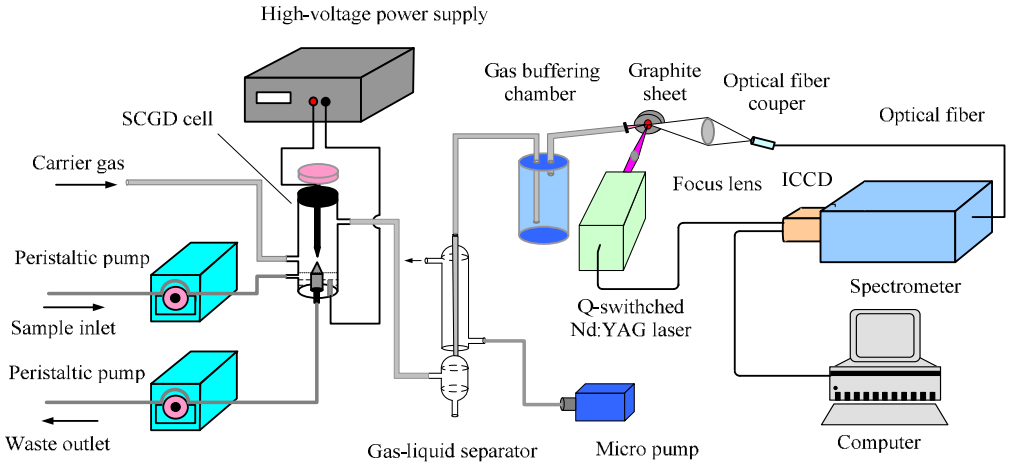

Fig.1 Schematic diagram of the experimental setup.

JAAS

RSCPublishing

PAPER

Online mercury determination by laser-induced breakdown spectroscopy with assistance of solution cathode glow discharge

Cite this: DOI: 10.1039/xoxxoooooox

Received ooth January 2012,
Accepted ooth January 2012

DOI: 10.1039/xoxxoooooox

www.rsc.org/

Peichao Zheng,*[a] Hongdi Liu,[a] Jinmei Wang,[a] Minjie Shi, [a] Xiaomeng Wang[a], Bin Zhang [a] and Rui Yang [a]

The trace mercury in aqueous solution is determined by laser-induced breakdown spectroscopy (LIBS) under the assistance of solution cathode glow discharge (SCGD) system. The aqueous solution is converted to gas phase using high voltage DC discharge, and then the generated mercury vapor is cooled by gas-liquid separator to improve the concentration of mercury. Finally, a 1064 nm wavelength Nd: YAG laser is used to produce plasma. In the present experiment, the characteristic spectral line of Hg I 253.65 nm is selected for analysis, under the optimal conditions of LIBS, the influences of the acid anion, discharge current, sample flow rate and carrier gas flow rate are investigated. The temporal behavior of the electron temperature and electron number density are also investigated, the results show that the electron temperature decreases from about 10900 K to 8800 K with delay time from 200 ns to 6 μs, and the electron number density is on the orders of 10^{17} and 10^{18} cm^{-3}, and it decreases with delay time. The analytical performances of this method are evaluated under optimized conditions, the calibration curve of Hg is plotted based on the different concentrations measurement results, and the detection limit (LOD) of Hg is calculated to be 0.36 $mg \cdot L^{-1}$. By using this experimental configuration, the detection limit and sensitivity of Hg are improved to some extent. This method provides an alternative analytical method for measurement of trace mercury in water.

Introduction

Nowadays, environmental pollution problems become more and more serious, and heavy metal pollution is a particular one. Various heavy metal pollution releasing from industry, traffic and domestic waste result in serious influence on environment and human's health.[1]Mercury is one of the most toxic and hazardous elements, which are durable, easy to transport and with high biological enrichment, any form of mercury can be converted into toxic methyl-mercury in certain conditions, mercury has been considered as a global pollutant due to its long residence time and mercury pollution has greatly increased in resent year. As a naturally occurring element, mercury can be found throughout the environment (soil, water, air) and can exist in three forms: elemental or metallic, inorganic, and organic.[2] For the characteristics mentioned above, there is an increasing concern about the determination and monitoring of mercury. Strict regulations for maximum allowable mercury concentration in environment and food samples have been established throughout the world, effective detecting methods are in urgent demand for corresponding supervision department.

In the past several decays, many detection methods have been proposed for the determination of mercury, and much efforts have devoted to improving the LOD of mercury because this element is usually present in food and water samples at extremely low concentrations. Hinds[3] developed a procedure to determine mercury in unrefined gold by flame and graphite furnace atomic absorption spectrometry (AAS). Grotti *et al.*[4] refined a procedure for the simultaneous determination of arsenic, selenium and mercury in foodstuffs by inductively coupled plasma-optical emission spectroscopy (ICP-OES). Pyhtilä *et al.*[5] developed and optimized a method for the determination of low total mercury concentrations in humic-rich natural water samples using cold vapor technique coupled to an inductively coupled plasma mass spectrometer (CV-ICP-MS). Hieftje group[6] developed a novel cold vapor generation method using solution cathode glow discharge (SCGD) coupled with ICP-OES in 2008. And then, He *et al.*[7] used the novel SCGD induced vapor generation as interface to on-line couple high-performance liquid chromatography (HPLC) with atomic fluorescence spectrometry (AFS) for the speciation of inorganic mercury, methyl-mercury and ethyl-mercury. Besides, the analytical performance including the figures of merit of those methods have been improved and developed.

Recently, laser-induced breakdown spectroscopy (LIBS) has aroused wide interest for its outstanding advantages such as rapid analysis, minimal sample preparation, practically non-destructive, operational simplicity, real-time analysis, and versatile sampling of solids, liquids, gases, or aerosols over conventional spectrometric analytical methods.[8] One of the most important applications of LIBS is the determination of trace amount of heavy metals in water and

food for environmental monitoring. Several achievements and improvements have been made in recent years, *e.g.* Pavan *et al.*[9] compared two potential spectroscopic methods (LIBS and spark induced breakdown spectroscopy (SIBS)) at their optimum experimental conditions for mercury monitoring. The LOD for mercury in soil calculated using LIBS and SIBS is 483 ppm and 20 ppm, respectively. Sobral *et al.*[10] investigated the detection sensitivity of trace Hg in water and ice samples by using laser-induced breakdown spectroscopy, the obtained LOD from water and ice samples are of the order of 21.4 ppm and 3.7 ppm, respectively. Fang *et al.*[11] directly and quantitatively compared two different sample presentation methods, plasma excitation within water bulk and on the surface in a water jet by LIBS, and the LOD of Hg obtained is in the order of 85 ppm. The main drawback of the LIBS used for the determination of mercury in aqueous solution is the limited sensitivity which is typically within the low numbers of the ppm range, thus the measurement should be taken to improve the sensitivity and stability of this technique.

In the present work, a novel procedure for the determination of the trace mercury in aqueous solution was developed based on LIBS. Dissolved mercury species have been converted to volatile Hg vapor by SCGD to improve the sensitivity of the determination of Hg. In addition, the influences of background electrolyte, discharge current, sample flow rate and carrier gas flow rate were investigated and optimized. The LOD of this method was estimated by using the calibration curve of Hg plotted based on the different concentration measurement results. The characteristic parameters of the plasma including the electron temperature and electron number density were investigated under different conditions, and it is shown that the local thermodynamic equilibrium (LTE) condition is fulfilled.

Experimental

Instrumental setup

The experimental setup is showed in Fig. 1. The detection system is sustained in an open-to-air atmosphere, and consists of three primary units: solution cathode glow discharge mercury vapor generator, gas-liquid separator (GLS) and LIBS equipment. A closed SCGD cell have been constructed and developed, in this design, a tapered tungsten rod was used as the anode, while the solution delivered through a customized quartz capillary with an internal diameter of 0.38 mm was the cathode, and the electrode gap of the discharge can be adjusted flexibly through the control knob. A high-voltage DC power supply (Yingkou high power research institute, GYU-015A) was used to ignite the discharge under the protection of power supply with a ceramic resistor (2.7 kΩ) used between the liquid anode and the positive output of the power supply. Sample solution was pumped into the cell via a peristaltic pump (Chongqing Jieheng pump Co. Ltd, BT-100), a portion of the solution not vaporized by the discharge overflows into a polytetrafluoroethylene (PTFE) waste reservoir during discharge, and this overflow provides an electrical connection between the discharge and the solution in the reservoir. The waste solution was drain out to maintain a constant solution level in the waste reservoir with the same peristaltic pump.

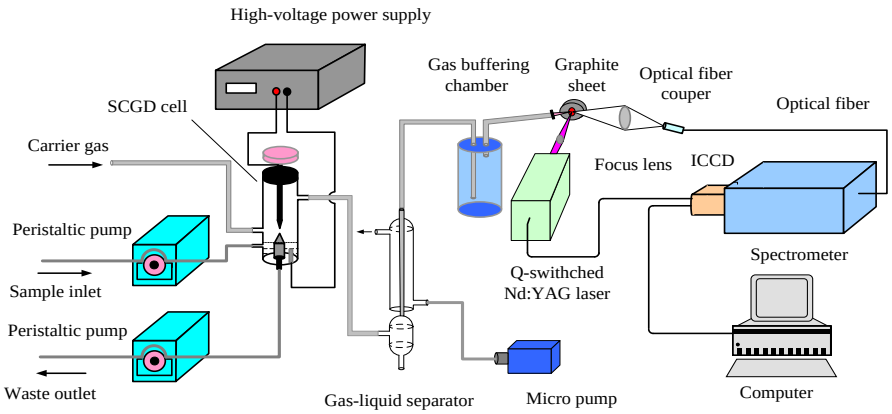

Fig.1 Schematic diagram of the experimental setup

When the Hg-containing sample was fed into the discharge cell, the volatile Hg vapor was produced. All generated products issuing from the plasma were swept by an air stream controlled by a rotor flowmeter. In order to improve the Hg concentration, the air flow containing Hg was then introduced to a GLS. The GLS was a condenser-based design consisting of two concentric tubes which was similar to the previously described.[12] The water-cooled condenser is 200 mm (length) ×6 mm (i. d.) ×20 mm (o. d.). The coolant water at approximate 4 ℃ circulating in the condenser was used. The vapor was then transported to a sealed container (400 mL) to reduce fluctuations of the gas flow rate. Finally the products were injected onto a graphite sheet through a 2 mm (i. d.) nozzle, the graphite sheet was used to adsorb the mercury vapor and improve the efficiency of laser ablation, and then the LIBS equipment was used for detection. A Q-switched Nd: YAG laser (Quantel, Ultra 100), at a fundamental wavelength of 1064 nm with a pulse duration of 8 ns, repetition rate of 20 Hz and maximum pulse energy of 100 mJ, was used as the excitation light source. The laser was focused on the surface of the graphite sheet by a 100 mm focal length plano-convex lens to produce intense, transient plasma. The light emitted from the plasma was collected by an optical signal collection device composed of two quartz lens and transported by a 2 m long multimode silica optical fiber. The light signal was then transmitted to the entrance of a computerized Czerny-Turner spectrograph (Andor Model SR-750A). The spectrograph is equipped with three ruled gratings: 2400 grooves/mm, 1200 grooves/mm, 300 grooves/mm, which can be changed according to different demands under the control of computer, it can provide high and low resolution spectra in the wavelength range of 200–1200nm. A 2048×512 pixels intensified and gated CCD camera (Andor DH340T-18U-03) was attached to the output end of the spectrograph to detect the spectrally resolved lines. The ICCD camera was cooled to -15 ℃ by Peltier cooler to reduce noise. Kept moving the three-dimension translation stage to make each fresh spot ablated during the experiment.

Reagents and solutions

In this work, the purity deionized water (17.1 MΩ·cm) was used throughout the experiment, single element solutions of Hg were prepared by appropriate dilutions of the stock of Hg standard

solution (1000 mg·L^{-1}). Superior-reagent grade HNO_3, H_2SO_4 and HCl were purchased from Chongqing Chuandong Chemical Group Co., Ltd. These commercial products were used to investigate the effect of different background electrolyte on the oxidation of mercury.

Stock solutions (1000 mg·L^{-1}) of Hg^{2+} was prepared by dissolution of appropriate masses of Mercuric chloride (99.5%). And all sample solutions were prepared in dilute nitric acid with the final PH adjusted to 1.0 after optimization.

Results and discussion

Fig.2 depicts a typical emission spectrum of liquid sample of $HgCl_2$ recorded for 10 mg·L^{-1} at the discharge current of 80 mA, discharge voltage of 1200 V, and the sample flow rate of 8.7 mL·min^{-1}. Besides the optimal parameters of LIBS were obtained by the sequential test method,[13] they are 0.4 μs ICCD delay, 10 μs gate width and 32 mJ laser pulse energy. As shown in Fig.3, in the range from 248 nm to 258 nm, and the spectral line of Hg I 253.65 nm is the most outstanding among all the spectral lines, therefore this line was selected for qualitative and quantitative analysis for the subsequent experiment.

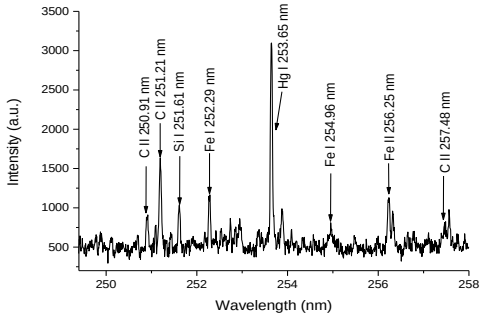

Fig.2 Typical LIBS spectra of vapor Hg in the range from 248 nm to 258 nm

In addition, the lines of C II 250.91 nm, 251.21 nm and 257.48 nm, and other impurities in graphite sheet such as Fe I 252.29 nm, 254.96 nm and Fe II 256.25 nm, Si I 251.61 nm obviously have been resolved. The spectral information of the above lines for qualitative and quantitative analysis was obtained from the NIST[14] database. Twenty pulses were accumulated to obtain each spectrum, and five such spectra were measured for each experimental condition in order to increase the sensitivity and reduce the standard deviation.

Effect of the acid anion

At the outset, the influences of background electrolyte, discharge current, sample flow rate and carrier gas flow rate on the emission intensity of mercury were studied, and then optimize these parameters to improve the detection sensitivity. The background electrolyte can affect the Hg vapor generation efficiency according to previous literature.[15] Thus, it's essential to investigate the effect of the acid anion on the mercury vapor generation to sustain high effective discharge. Three mercury standard solutions (concentration of 10 mg·L^{-1}) were adjusted to a PH of 1.0 with the acids: Sulfuric acid, hydrochloric acid and nitric acid, passed them into the discharge system, respectively. The discharge voltage was kept constant at 1200 V for all solution. The solution flow rate and carrier gas flow rate were 8.7 mL·min^{-1} and 300 mL·min^{-1}, respectively. It was observed that all of these acidic media could sustain the stability of discharge and mercury could be easily transformed into volatile mercury species by this device. Different degree enhancement in sensitivity over conventional water jet LIBS was obtained. Different acid anions present varied effects on the emission intensity due to the analyte, which is showed in Fig.3. The sample acidized by HNO_3 results in the maximum intensity and minimum background emission, and the order of enhancing signal intensity is HNO_3> H_2SO_4> HCl. In addition, nitric acid is the preferred reagent for digestion of samples and has the chemical compatibility. Accordingly, nitric acid (PH=1) is selected as acidic medium for our subsequent experiment.

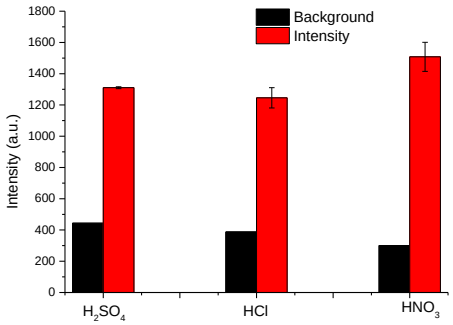

Fig.3 Effect of acid anion on emission signal of Hg I 253.65 nm

Effect of discharge current

The influence of the discharge current on stable operation and vapor generation efficiency was also evaluated to obtain maximum sensitivity of emission intensity. Adjusted the discharge current from 40 to 110 mA, other parameters of this detection system were the same as before. The emission intensity of Hg I 253.65 nm variation with discharge currents is illustrated in Fig.4. The result shows obviously that the intensity of Hg atomic emission becomes stronger with the increasing of discharge current, which indicates that the vapor generation efficiency of Hg increase with the increasing of discharge currents. Maybe it's the consequence of the high discharge power enhances both reduction and volatilization efficiency. However, when the current is high enough, excessive heating of the anode takes place and the temperature turns to extremely high, and the discharge plasma became unstable, and worse of all, it was more energy-consuming. Taking all factors above into consideration, a discharge current of 80 mA was employed in the remaining parts of the experiment.

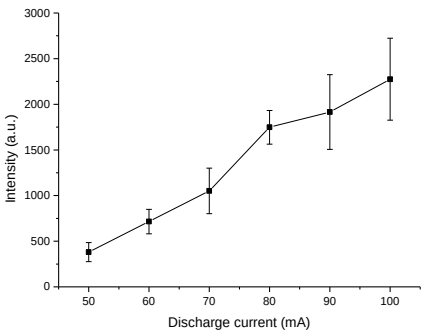

Fig.4 Emission intensity of Hg I 253.65 nm as a function of discharge currents

Effect of sample flow rate

In order to improve the efficiency of determination, and reduce sample consumption, the effect of solution flow rate on the signal was evaluated in the range of 5.8-12.8 mL·min^{-1} (Fig. 5). The flow liquid cathode was the Hg solution of 10 mg·L^{-1}, and the flow rate of air used to carry the Hg vapor sample was 300 mL·min^{-1}. The increase in the flow rate of the liquid cathode solution was also effective. The maximum signal was obtained by using the liquid flow rate of 8.7 mL·min^{-1}. The atomic emission intensity increased with the liquid flow rate from 5.8 to 8.7 mL·min^{-1} mainly because of the raised amount of analyte that entered the discharge. When the flow rate was too low (<5.8 mL·min^{-1}), the discharge was unstable and easy to extinguish. However, it was found that, too high solution flow rate resulted in lower signal of Hg emission. This might be caused by the changing of SCGD plasma, which decreased Hg vapor generation efficiency. Additionally, the increasing water vapor pressure at high flow rate may also cool the laser-induced plasma. The stability of signal at the liquid flow rate of 8.7 mL·min^{-1} seems worse than others which may due to the transition of liquid flow rate from 7.27 to 8.7 mL·min^{-1}, while from the trend of signal intensity, the highest signal is obtained at the liquid flow rate of 8.7 mL·min^{-1}. Based on these results, a flow rate of 8.7 mL·min^{-1} was selected in the following experiment.

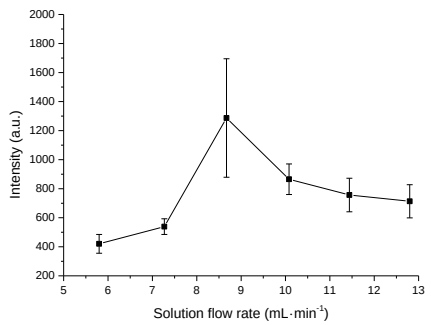

Fig.5 Emission intensity of Hg I 253.65 nm as a function of solution flow rate

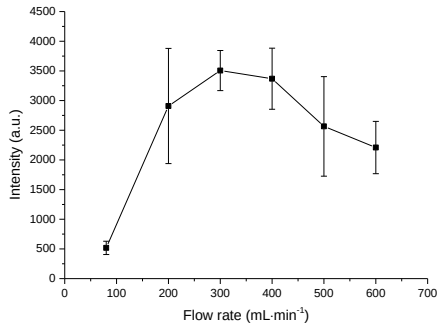

Fig.6 Emission intensity of Hg I 253.65nm as a function of carrier gas flow rate

Effect of carrier gas flow rate

To enable the experimental system's universality and simplify the detection device, the air was used as the carrier gas during the whole experiment. The influence of flow rates of the carrier gas were investigated in the range of 80-600 mL·min^{-1} on the basis of the spectral intensity from a 10 mg·L^{-1} Hg solution. The volatile mercury species produced in the SCGD were brought to the LIBS equipment for determination through the carrier gas. The variation of the signal intensity as a function of carrier gas flow rate is shown in Fig.5. It is observed that emission intensity increases to the maximum signal with the increasing of carrier gas flow rate and decreases afterwards, the highest signal is obtained at the carrier gas flow rate of 300 mL·min^{-1}. Accordingly, a flow rate of 300 mL·min^{-1} was employed in the remaining part of the experiment.

Calibration curve and limit of detection

In the LIBS method, a calibration curve is the most widely used technology for quantitative analysis. For construction of the calibration curve, several standard solutions with different concentrations have been prepared through dissolving $HgCl_2$ in known volumes of de-ionized water. The aqueous solutions with different concentrations ranging from 100 μg·L^{-1} to 10 mg·L^{-1} were prepared, and the calibration curve is shown in Fig.7.

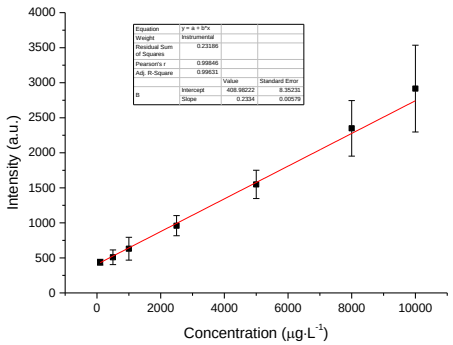

Fig.7 Experimental calibration curve of emission intensity of Hg I 253.65 nm versus the Hg concentration

The LOD is defined as the lowest concentration that can be detected and is evaluated by [16]:

$$LOD = \frac{3\sigma}{S} \quad (1)$$

Where σ is the standard deviation of the background emission and S is the slope of calibration curve. In this experiment, σ is the standard deviation of the background calculated from 30 replicated determinations with an analytical blank within the spectral range of the related peak. Finally, the LOD of Hg I 253.65 nm by the proposed method is determined to be 0.36 mg·L^{-1}, which is about two orders of magnitude lower than the results of previous literatures.[9,17] The reason for the improving of the detection sensitivity is mainly due to the vapor generation and concentrating of the aqueous solution.

Compared with other works about the determination of mercury based on LIBS technology, our work improved the sensitivity in some extent. The comparison between this work and resent results is summarized in table 1.

Table 1 Comparison of the trace mercury limit of detection obtained from different detection

Detection methods	Species	Wavelength(nm)	LOD (ppm)
SCGD-LIBS (this work)	Hg I	253.65	0.36
Single LIBS(liquid sample) [10]	Hg I	253.65	21.4
Single LIBS (evaporated in a carbon planchet)[17]	Hg I	253.65	10
Single LIBS(water jet)[11]	Hg I	253.65	85
Single LIBS and	Hg I	546.07	483
SIBS (soil sample)[9]			20
OEDP-LIBS [18]	Hg I	253.65	0.3

Measurements of electron temperature and electron number density

Since the sample was converted to gas phase from aqueous solution, and then used the LIBS to detect the toxic metal Hg, it's necessary to know the properties (electron temperature and electron number density) of the laser induced mercury vapor plasma. Besides, the quantitative analysis of this experiment was based on the assumption of local thermodynamic equilibrium (LTE), thus it's essential to show the validity of this assumption, in the following subsections, electron temperature, electron number density and LTE are discussed.

The plasma parameters represent the most fundamental physical quantities, whose knowledge is useful for characterization of the plasma and its efficient used for analytical purposes.[19] Electron temperature (T) is one of the most important properties of any excitation sources, and its determination is important to understand the dissociation, ionization and excitation process taking in the plasma.[20] Two methods have been applied to determine T, namely the Boltzmann plot method and the line pair ratio method from the relative intensities of observed lines. The result obtained through the Boltzmann plot method is more accurate than the line pair ratio due to more spectral lines are used to extract T. Therefore, the Boltzmann plot method was selected to determine the electron temperature in this work. Assuming the LTE is established within the plasma, the population in different levels is governed by the Boltzmann distribution. The following relation has been used to extract the electron temperature.[21]

$$\ln\left(\frac{I_{ki}\lambda_{ki}}{A_{ki}g_k}\right) = -\frac{E_k}{k_B T} + \ln\left(\frac{N(\mathrm{T})}{U(\mathrm{T})}\right) \quad (2)$$

Where k_B is the Boltzmann constant, $U(T)$ is the partition function, I_{ki} is the integrated line intensity of the transition involving an upper level (k) and lower level (i), λ_{ki} is the transition wavelength, A_{ki} is the transition probability, g_k is the statistical weight of level (k), $N(T)$ is total number density, and E_k is the energy of upper level. Eq. (2) leads to a liner plot of ln ($\lambda_{ki}I/A_{ki}g_k$) versus the term energy E_k, and the electron temperature can be deduced from the slope of the fitting straight line. Thus the electron temperature can be determined without the knowledge of total number density or the partition function.

In this work, the gate width of the ICCD is 200 ns and the laser pulse energy is 32 mJ. Other spectral lines *i.e.* C I, Ca II and Ca I are significant. The spectral lines of Ca II 317.93 nm, Ca II 370.60 nm, Ca II 373.69 nm, Ca II 393.37 nm and Ca II 396.85 nm are selected to extract the electron temperature. The LIBS spectrum of plasma in the range of 315-400 nm containing the lines of Ca II is illustrated in Fig.8. The measured intensities of spectral lines and other spectroscopic data such as wavelength (λ), statistical weight (g), transition probability (A) and term energy (E) listed in the table 2.

Table 2 Spectroscopic parameters of the Ca II lines

Sr. No.	Wavelength λ(nm)	Transitions	Statistical weight g_k	Transition probability A_{ki}(s^{-1})	Energy(eV)	
					E_k	E_i
1	317.93	$3p^6 4d\,^2D_{3/2} \rightarrow 3p^6 4p\,^2P^0_{1/2}$	6	3.6×10^8	7.049150	3.150984
2	370.60	$3p^6 5s\,^2S_{1/2} \rightarrow 3p^6 4p\,^2P^0_{1/2}$	2	8.8×10^8	6.467875	3.123349
3	373.69	$3p^6 5s\,^2S_{1/2} \rightarrow 3p^6 4p\,^2P^0_{3/2}$	2	1.7×10^8	6.467875	3.150984
4	393.37	$3p^6 4p\,^2P^0_{3/2} \rightarrow 3p^6 4s\,^2S_{1/2}$	4	1.47×10^8	3.150984	0
5	396.85	$3p^6 4p\,^2P^0_{1/2} \rightarrow 3p^6 4s\,^2S_{1/2}$	2	1.4×10^8	3.123349	0

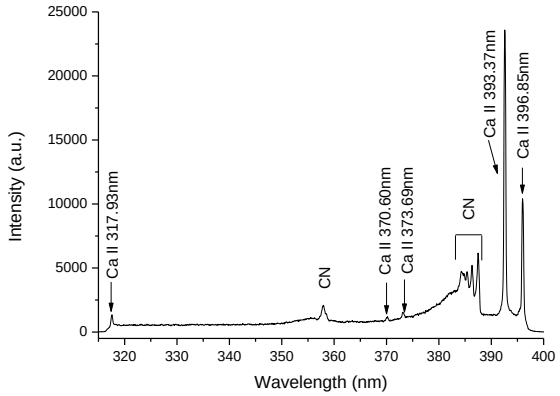

Fig.8 LIBS spectra of vapor Hg in the range of 315-400 nm

Fig.9 shows the Boltzmann plot obtained from Ca ionic lines, where the curved slope yields the electron temperature. The electron temperatures obtained as a function with the ICCD delay time can be calculated from the slopes of the corresponding Boltzmann's plots, the result is illustrated in Fig.10. As can be seen, the electron temperature decreases with ICCD delay time from about 10900 K to 8800 K when the delay time range from 200 ns to 6 μs.

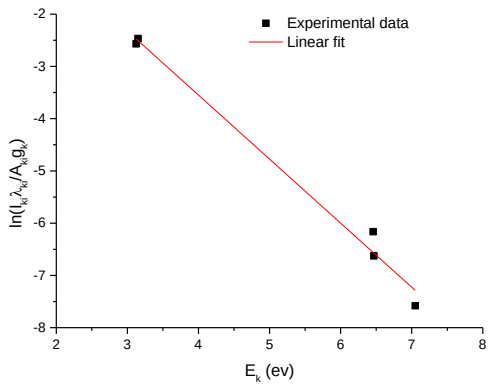

Fig.9 A Boltzmann plot built using the emission lines of Ca II

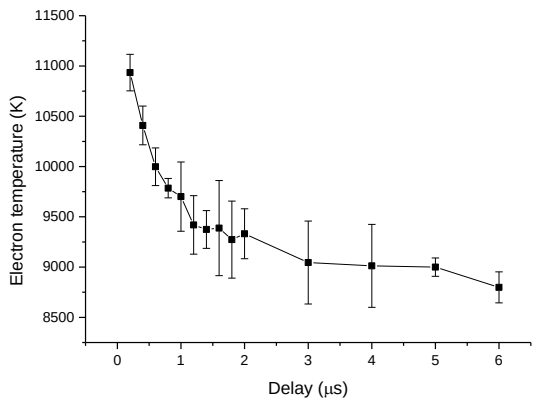

Fig.10 Temporal behavior of electron temperature with Hg (II) solution at a concentration of 10 mg·L^{-1}

During the evolution of laser induced plasma, excitation and ionization of the evaporated material occur. The electron number density is a crucial parameter for determining the elemental composition. In fact, there are two main line broadening mechanisms in laser induced plasma, *i.e.* Stark broadening and Doppler broadening. At high plasma density, Stark broadening induced by collision with charged particles dominates. One of the most reliable techniques to determine the electron number density is from the measured Stark broadened line profile of an isolated line of either neutral atom or single charged ion. The full width at half maximum (FWHM) $\Delta\lambda_{1/2}$ of a line given by the following relation[21]

$$\Delta\lambda_{1/2} = 2\omega\left(\frac{N_e}{10^{16}}\right) + 3.5A\left(\frac{N_e}{10^{16}}\right)^{1/4}\left[1 - 1.2N_D^{-1/3}\right]\omega\left(\frac{N_e}{10^{16}}\right) \quad (3)$$

Where ω is the electron impact width parameter, A is the ion broadening parameter, N_D is the number of particles in the Debye sphere, and N_e is the electron number density. The first term on the right side comes from the electron interaction, while the second one is generated by the ion interaction. Since the contribution of the ionic broadening is very small as compared to the Stark broadening due to plasma electrons and ions, therefore, it can be neglected. The relation between electron number density and $\Delta\lambda_{1/2}$ of Stark broadened line can be expressed by following expression:

$$\Delta\lambda_{1/2} = 2\omega\left(\frac{N_e}{10^{16}}\right) \quad (4)$$

In this work, the electron number density (N_e) is calculated by the measurement of the FWHM of Stark broadened Voigt line shape of the ionic line (393.37 nm) of Ca II (Fig.11).The value of ω corresponding to different electron temperatures can be obtained from the reference data[22].

The temporal behavior of the electron number density obtained from the Ca II 393.37 nm is shown in Fig.12. As Fig.12 shows, electron number density of the plasma is on the order of 10^{18} cm^{-3}, and it decreases with ICCD delay time to 10^{17} cm^{-3} due to the recombination of free electrons and ions.

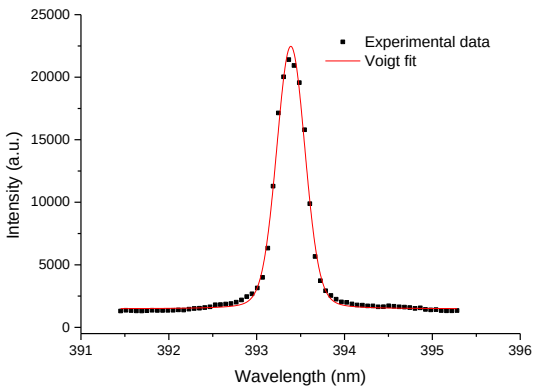

Fig.11 Voigt plot for the single ion line Ca II 393.37 nm

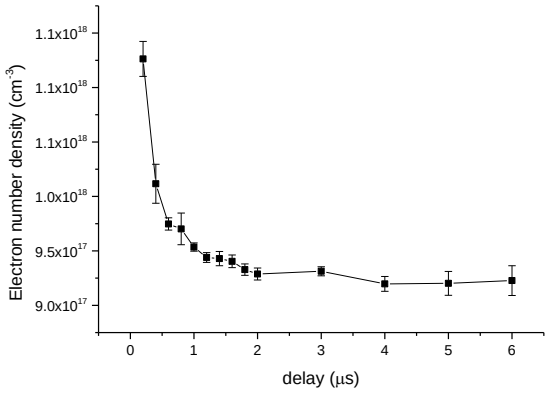

Fig.12 Temporal behavior of electron number density with Hg (II) solution at a concentration of 10 mg·L^{-1}

The use of the emission spectroscopy for the determination of the electron temperature and electron number density requires optically thin spectral lines. The self-absorption depends on the oscillator strength, level energy degeneracy, broadening parameters and also on the plasma parameters.[23] The laser induced plasma is observed to be optically thin as in case of self-absorption a strong line appears to have a dip in the central frequency (self-absorption).[22] In the present work we did not find any dip at the central frequency of the observed emission lines. Since it is assumed in our experiment that the plasma is described by the local thermodynamic equilibrium (LTE). The necessary condition for LTE that gives the corresponding lower limit of the electron density Ne is given by Mcwhirter criterion[24]

$$N_e \geq 1.6 \times 10^{12} T^{1/2} (\Delta E)^3 \quad (5)$$

Where ΔE (eV) is the highest energy transition for which the condition holds, and $T(K)$ is the electron temperature. In our experiment, the electron temperature ranges from 8799 K to 10934 K, and ΔE= 3.8986 eV. The lower limit of given by Eq. (5) is 9.9×10^{16} cm^{-3}, while the electron number density in our work is on the order of 10^{17} and 10^{18} cm^{-3}. Therefore, the assumption of LTE is demonstrated.

Conclusions

Analysis of toxic metal of mercury in aqueous solution $HgCl_2$ was carried out by laser-induced breakdown spectroscopy under the assistance of solution cathode glow discharge. The liquid sample is converted to gas phase through high voltage DC discharge, and then the generated mercury vapor is concentrated by the GLS. Finally, a 1064 nm wavelength Nd: YAG laser was used as excitation source to ignite the plasma, and the high resolution Czerny-Turner spectrometer and ICCD detector were used for spectral separation and detection. The characteristic spectral line of Hg I 253.65 nm was selected for analysis, under the optimal conditions of LIBS, the optimal and proper acidification reagent, discharge current, sample flow rate and carrier gas flow rate were determined through the investigation. The analytical performances of this method are evaluated under optimized conditions, the calibration curve of Hg is plotted based on the different concentration measurement results, and the LOD of Hg is calculated to be 0.36 mg·L^{-1}. Besides the temporal behavior of electron temperature and electron number density were investigated, the results show that the electron temperature decreases from about 10900 K to 8800 K with the delay time from 200 ns to 6μs, and the electron number density is on the orders of 10^{17} and 10^{18} cm^{-3}, it decreases with delay time due to the recombination of free electrons with ions. By using this experimental configuration, the detection limit and sensitivity of Hg are improved to some extent. This method provides an alternative analytical method for measurement of trace mercury in water.

Acknowledgements

This work was financially supported by the National Natural Science Foundation of China (61205149), Scientific and Technological Talents Training Project of Chongqing (CSTC2013kjrc-qnrc40002), 2013 Program for Innovation Team Building at Institutions of Higher Education in Chongqing (The Innovation Team of Smart Medical System and Key Technology), and Scientific and Technological Project of Nan'an District.

Notes and references

[a] College of Optoelectronic Engineering, Chongqing University of Posts and Telecommunications, Chongqing Municipal Level Key Laboratory of Photoelectronic Information Sensing and Transmitting Technology, Chongqing 400065, P. R. China. E-mail: zhengpc@cqupt.edu.cn; Fax: +86-23-62460592; Tel: +86-23-62460592

1 Z. Wang, Y. Deguchi, M. Kuwahara, X. Zheng, J. Yan and J. Liu, *Japan. J. Appl. Phys.*, 2013, **52,** 11NC05 (1)-11NC05 (6).
2 S. Mostafalou, M. Abdollahi, *Archives of Industrial Hygiene and Toxicology*, 2013, **64,** 179-181.
3 M. W. Hinds, *Spectrochim. Acta, Part B*, 1998, **53,** 1063-1068.
4 M. Grotti, C. Lagomarsino, E. Magi, *Annal. Chim.*, 2006, **96,** 751-764.
5 H. Pyhtilä, P. Peräniki, J. Piispanen, M. Niemelä, T. Suoranta, M. Starr, T. Nieminen, M. Kantola and L. Ukonmaanaho, *Microchem. J.*, 2012, **103,** 165-169.
6 Z. Zhu, G. C. Y. Chan, S. J. Ray, X. Zhang and G. M. Hieftje, *Anal. Chem.*, 2008, **80,** 7043-7050.
7 Q. He, Z. Zhu, S.Hu and L. Jin, *J. Chromatogr. A*, 2011, **1218,** 4462-4467.
8 P. Zheng, H. Liu, J. Wang, B. Yu, B. Zhang, R. Yang and X. Wang, *Anal. Methods*, 2014, **6,** 2163-2169.
9 P. K. Srungaram, K. K. Ayyalasomayajula, F. Yu-Yueh and J. P. Singh, *Spectrochim. Acta, Part B*, 2013, **87,** 108-113.
10 H. Sobral, R. Sanginés, A. Trujillo-Vázquez. *Spectrochim. Acta, Part B*, 2012, **78,** 62-66.
11 X. Fang, S. Rafi Ahmad, *Appl. Spectrosc.*, 2007, **61,** 1021-1024.
12 Z. Zhu, C. Huang, Q. He, Q. Xiao, Z. Liu, S. Zhang and S. Hu, *Talanta*, 2013, **106,** 133-136.

13 P. Zheng, H. Liu, J. Wang, K. Liu, Y. Dai, B. Yu, B. Zhang, R. Yang and X. Wang, *High Power Laser and Particle Beams*, 2013, **25,** 2729-2733.
14 http://physics.nist.gov/PhysRefData/ASD/lines_form.html.
15 Z. Zhu, Q. He, Q. Shuai, H. Zheng and S. Hu, *J. Anal. At. Spectrom.*, 2010, **25,** 1390-1394.
16 M. Sabsabi, P. Cielo, *Appl. Spectrosc.*, 1995, **49,** 499-507.
17 R. L. V. Wal, T. M. Ticich, J. R. West, P. A. Householder, *Appl. Spectrosc.*, 1999, **53,** 1226-1236.
18 Q. Zhang, W. Xiong, Y. Chen, and R. Li, *Spectroscopy and Spectral Analysis*, 2011, **31,** 521-524.
19 A. A. I. Khalilm, *Opt. Laser Techno.*, 2013, **45,** 443-452.
20 M. Hanif, M, Salik, M. A. Baig, *Journal of Modern Physics*, 2012, **3,** 1663-1669.
21 M. Hanif, M. Salik, M. A. Baig, *Opt. Spectrosc.*, 2013, **114,** 7-14.
22 H. R. Griem, Plasma spectroscopy, McGraw-Hill, New York, 1964.
23 M. Hanif, M. Salik, M. A. Baig, *Plasma Sci. technol.*, 2011, **13,** 129-134.
24 R. W. P. McWhirter, R. H. Huddlestone, S. L. Leonard, *Plasma diagnostic techniques*, Academic, New York, 1965.